Chapter 4

The Rabi Hamiltonian

In this chapter, we discuss the analytic limits of the Rabi Hamiltonian, and benchmark the numerical diagonalization results for the Rabi spectrum against known analytic results. We investigate the physical nature of the Rabi ground state, and present a review of some existing results for the ground and first excited states obtained via many–body methods other than the CCM.

4.1 Discussion of the Rabi Hamiltonian

The Rabi Hamiltonian

$$\begin{aligned} H_{\text{Rabi}} &= \frac{1}{2}\omega_0\,\sigma^z + \omega\, b^\dagger b + \eta\,\left(b^\dagger + b\right)\sigma^x \\ &= \frac{1}{2}\omega_0\,\sigma^z + \omega\, b^\dagger b + g\,\left(b^\dagger + b\right)\left(\sigma^+ + \sigma^-\right)\,, \end{aligned} \tag{4.1}$$

where $\eta = 2g$, and its conserved parity

$$\Pi_{\text{Rabi}} \;=\; \exp\{i\pi N\}\,, \qquad N \;=\; b^\dagger b + \frac{1}{2}\,(\sigma^z + 1)\;, \tag{4.2}$$

were introduced in Chapter 2. Given that most recent interest in the Rabi Hamiltonian is in the field of quantum optics, we present our analysis of the Hamiltonian in this context. In typical optical applications, the coupling g is small, and the so–called counter–rotating terms $g\left(b^\dagger\sigma^+ + b\sigma^-\right)$ in the Hamiltonian (4.1), corresponding respectively to the processes where a photon is created as the atom makes an upward transition and where a photon is annihilated as the atom makes a downward transition, may to good approximation be neglected. This rotating wave approximation (RWA) results in the well–known Jaynes–Cummings Hamiltonian [Ja63]

$$H_{\text{JC}} \;=\; \frac{1}{2}\omega_0\,\sigma^z \;+\; \omega\, b^\dagger b \;+\; g\, b^\dagger\sigma^- \;+\; g\, b\sigma^+\,. \tag{4.3}$$

In the Jaynes–Cummings model $[H_{\text{JC}}, N] = 0$ and the model is exactly soluble, since we may diagonalize H_{JC} in each subspace labelled by a fixed number, say n, of quanta. For $n = 0$, there is only one state, namely the product state $|0\rangle|\downarrow\rangle$, where the first ket refers to the field mode in the occupation number (Fock) representation and the second denotes the atomic state with the atom in its lower level, corresponding to energy $E^{\text{JC}}_{0,-} = -\frac{1}{2}\omega_0$ where the notation is convenient in what follows. For $n \geq 1$, the states $|n\rangle|\downarrow\rangle$ and $|n-1\rangle|\uparrow\rangle$ form a basis for the subspace corresponding to a given n, and one may diagonalize the resulting set of 2×2 matrices to obtain

$$E^{\text{JC}}_{n,\pm} = \omega\left(n - \frac{1}{2}\right) \pm \frac{1}{2}\sqrt{(\omega - \omega_0)^2 + 16ng^2} \qquad (n \geq 1)\,. \tag{4.4}$$

Since $E^{\text{JC}}_{n,+} > 0 > E^{\text{JC}}_{0,-}\ \forall\ n \geq 1$, the ground–state energy of H_{JC} is given, at each value of the coupling g, by the smallest element of the set $\{E^{\text{JC}}_{n,-}, n \geq 0\}$.

The corresponding eigenstates are often referred to as "dressed" states in quantum optics, where they are utilized in the study of, amongst others, the time development of the system given particular initial conditions for the atom and field [Mi91, Sh93], and the quasiperiodic recurrence phenomena of collapse and revival which characterize the Jaynes–Cummings model [Na88, Ge90, Mi91, Sh93].

The more general Rabi Hamiltonian (4.1), which extends the Jaynes–Cummings model beyond the RWA, is of interest for a variety of reasons. Given that quantum optics experiments are nowadays being performed with ever–increasing field intensities [An94], there is considerable agreement (see, *e.g.*, [Cr91, Fe96, Lo98]) that the full Rabi Hamiltonian merits investigation. Furthermore, it is known (see [Mi83] and references therein) that quantum chaotic behaviour does not occur in the RWA. Although there is no consensus as to whether the Rabi Hamiltonian does exhibit chaotic behaviour [Gr84a, Ku85, Ei86, Mi91], it is clear that the counter–rotating terms are essential if the possibility of quantum chaos is to exist. Finally, Hamiltonians similar to (4.1) occur in the theory of vibronic interactions [Berb] and in the analysis of a quantum tunneling system under the influence of a phonon bath [Le87], as well as in the study of the two–site polaron Hamiltonian in solid state physics [Mah].

The strict limitation of the fermionic subsystem of the Rabi model to two levels represents an idealization which, from a physical point of view, may generally only be regarded as realistic for $\omega_0 \simeq \omega$. For large atom–field detuning, one might reasonably expect that effects due to the multilevel

nature of the true atomic system would be at least as important as those due to the non–rotating terms included in (4.1); in most of what follows we will therefore focus on the case of resonance. It is then convenient to scale out the ω–dependence by setting $\omega = \omega_0 = 1$, and we will refer to the resulting Hamiltonian as the scaled resonant Rabi Hamiltonian.

4.1.1 Exact limits of the Hamiltonian

The Rabi Hamiltonian is analytically soluble in two limits, namely that of zero coupling ($g = 0$), and that of degenerate electronic levels ($\omega_0 = 0$). For zero coupling and nondegenerate atomic levels ($\omega_0 > 0$), the exact ground state assumes the form $|0\rangle|\downarrow\rangle$, and the corresponding ground–state energy is given by $E_0^{g=0} = \frac{-\omega_0}{2}$. Note that, in this case, the ground state is unique and of positive parity.

The case of nonzero coupling and degenerate atomic levels is important because, as we will demonstrate below, the Hamiltonian with a finite value for ω_0 approaches this case as $g \to \infty$. For $\omega_0 = 0$, $\left[H_{\text{Rabi}}^{\omega_0=0}, \sigma^x\right] = 0$, so that the eigenstates of $H_{\text{Rabi}}^{\omega_0=0}$ may be taken to be eigenstates of σ^x, and we obtain

$$H_{\text{Rabi}}^{\omega_0=0} = \omega\, b^\dagger b \pm 2\, g\, \left(b^\dagger + b\right) , \tag{4.5}$$

where the upper (lower) sign refers to the choice of the upper (lower) eigenstate of σ^x. The Hamiltonian (4.5) represents a shifted harmonic oscillator, as is easily seen by performing the canonical transformations (see *e.g.* [Hak])

$$\tilde{b}_\pm = b \pm \frac{2g}{\omega} , \qquad \tilde{b}_\pm^\dagger = b^\dagger \pm \frac{2g}{\omega} , \tag{4.6}$$

which preserve the bosonic commutation relations, to yield

$$H_{\rm Rabi}^{\omega_0=0} = \omega\, \tilde{b}_\pm^\dagger \tilde{b}_\pm - \frac{4g^2}{\omega}\,. \tag{4.7}$$

For the ground state $|\Psi\rangle$ of $H_{\rm Rabi}^{\omega_0=0}$,

$$\tilde{b}_\pm|\Psi\rangle = 0 \quad \Rightarrow \quad b|\Psi\rangle = \mp\frac{2g}{\omega}|\Psi\rangle\,. \tag{4.8}$$

Thus the (normalized) degenerate ground states $|\Psi_{01}\rangle$ and $|\Psi_{02}\rangle$ of the Rabi Hamiltonian for $\omega_0 = 0$ are the (normalized) coherent bosonic states

$$|\mp x\rangle = e^{-x^2/2}\exp\left[\mp x b^\dagger\right]|0\rangle = e^{-x^2/2}\sum_{n=0}^{\infty}\frac{(\mp x)^n}{\sqrt{n!}}|n\rangle\,, \tag{4.9}$$

with $x = 2g/\omega$, multiplied by the corresponding eigenfunctions of σ^x

$$\frac{1}{\sqrt{2}}\exp\left[\pm\sigma^+/2\right]|\downarrow\rangle = \frac{1}{\sqrt{2}}\left(|\downarrow\rangle \pm |\uparrow\rangle\right)\,, \tag{4.10}$$

and may thus be written as [Gr84b],

$$\begin{aligned}
|\Psi_{01}\rangle &= \frac{1}{\sqrt{2}}|-x\rangle\exp\left[\sigma^+/2\right]|\downarrow\rangle \\
&= \frac{1}{\sqrt{2}}e^{-2g^2/\omega^2}\exp\left[-\frac{2g}{\omega}b^\dagger\right]|0\rangle\ \left(|\downarrow\rangle + |\uparrow\rangle\right) \\
|\Psi_{02}\rangle &= \frac{1}{\sqrt{2}}|x\rangle\exp\left[-\sigma^+/2\right]|\downarrow\rangle \\
&= \frac{1}{\sqrt{2}}e^{-2g^2/\omega^2}\exp\left[\frac{2g}{\omega}b^\dagger\right]|0\rangle\ \left(|\downarrow\rangle - |\uparrow\rangle\right)\,,
\end{aligned} \tag{4.11}$$

with the ground–state energy in both cases given by $E_0^{\omega_0=0} = -4g^2/\omega$.

Having obtained the solution (4.11), we now demonstrate that the equivalence of the limits $\omega_0 \to 0$ and $g \to \infty$, although not formally proven, is at least consistent with this form of the solution. Heuristically treating the set of states $\{|\Psi_{01}\rangle, |\Psi_{02}\rangle\}$ as a basis for the full Rabi Hamiltonian (4.1) with

$\omega_0 > 0$, we obtain the matrix representation

$$\begin{bmatrix} -\frac{4g^2}{\omega} & -\frac{1}{2}\omega_0 e^{-8g^2/\omega^2} \\ -\frac{1}{2}\omega_0 e^{-8g^2/\omega^2} & -\frac{4g^2}{\omega} \end{bmatrix} \tag{4.12}$$

for H_{Rabi}. For finite g, the Hamiltonian couples the states $|\Psi_{01}\rangle$ and $|\Psi_{02}\rangle$ via the off–diagonal terms, and the diagonalization of (4.12) yields the two eigenenergies

$$E_{\pm} = E_0^{\omega_0=0} \mp \frac{1}{2}\omega_0 e^{-8g^2/\omega^2} , \tag{4.13}$$

with corresponding eigenfunctions

$$\begin{aligned} |\Psi_+\rangle &= \frac{1}{\sqrt{2}}\left(|\Psi_{01}\rangle + |\Psi_{02}\rangle\right) \\ |\Psi_-\rangle &= \frac{1}{\sqrt{2}}\left(|\Psi_{01}\rangle - |\Psi_{02}\rangle\right) . \end{aligned} \tag{4.14}$$

As $g \to \infty$ with ω_0 finite, the off–diagonal elements of the matrix (4.12) vanish exponentially. In this limit, the eigenfunctions (4.14), which are linear combinations of the states (4.11), thus become degenerate with energy $E_{\pm}^{g\to\infty} = E_0^{\omega_0=0}$, and the $\omega_0 = 0$ solution is reproduced. Furthermore, since

$$\Pi_{\text{Rabi}}|\Psi_{01}\rangle = |\Psi_{02}\rangle , \qquad \Pi_{\text{Rabi}}|\Psi_{02}\rangle = |\Psi_{01}\rangle , \tag{4.15}$$

we may write the states (4.14) in the form

$$\begin{aligned} |\Psi_+\rangle &= \frac{1}{\sqrt{2}}\left(1 + \Pi_{\text{Rabi}}\right)|\Psi_{01}\rangle \\ |\Psi_-\rangle &= \frac{1}{\sqrt{2}}\left(1 - \Pi_{\text{Rabi}}\right)|\Psi_{01}\rangle . \end{aligned} \tag{4.16}$$

Given that $\Pi_{\text{Rabi}}^2 = 1$, the states $|\Psi_+\rangle$ and $|\Psi_-\rangle$ are therefore of positive and negative parity, respectively. Also, the bosonic coherent states $|\pm 2g/\omega\rangle$ reduce to the bosonic vacuum $|0\rangle$ at $g = 0$, and the state $|\Psi_+\rangle$ ($|\Psi_-\rangle$), although not the exact ground (first excited) state at finite g, is therefore the analytic ground (first excited) state at $g = 0$.

4.1.2 Juddian solutions and the configuration–interaction (CI) method

Several attempts at an analytically exact treatment of the Rabi Hamiltonian have been made. There is very strong numerical support for the conjecture of Reik *et. al.* [Re86, Re87] involving generalized spheroidal wave functions, but a formal proof of the integrability of (4.1) is still missing (note here the work of Szopa *et. al.* [Sz96]). As demonstrated in the introduction to this chapter, the Jaynes–Cummings model, *i.e.* the Rabi Hamiltonian within the RWA, is analytically soluble. This result may also be obtained via a unitary Holstein–Primakoff mapping of both the fermionic and bosonic aspects of the Jaynes–Cummings Hamiltonian into a system composed of two ideal boson modes, where the resulting bosonized Hamiltonian may be solved exactly [Ci98] [1]. This success of this bosonization approach, however, depends crucially on the fact that H_{JC} commutes with the number operator N introduced in (4.2), while $[H_{\mathrm{Rabi}}, N] \neq 0$.

However, isolated analytic solutions for some of the higher lying states in the spectrum of the Rabi Hamiltonian are known. These solutions were first obtained for a class of Jahn–Teller systems by Judd [Ju79], who established explicit finite order equations for the isolated values of the coupling at which the Jahn–Teller eigenvalues can be determined analytically, and these isolated exact solutions are thus known as Juddian solutions. Subsequently, Reik *et.al.* [Re82] showed that the Juddian solutions for the Rabi Hamiltonian

[1] See also the non-unitary Dyson boson mapping technique employed in [Ca87], albeit to a different Hamiltonian.

may be obtained as a special case of those for the linear $E \otimes e$ pseudo Jahn–Teller model. A fuller discussion of the approach taken by Reik *et.al.* is thus deferred to Chapter 7. Here we simply point out that the values of the coupling g for which Juddian solutions for the Rabi system occur are given [Re82] by the solutions of

$$A_N + B_N = 0 \tag{4.17}$$

where $N \in \{0, 1, 2, \ldots\}$, and A_N and B_N are determined recursively via

$$\begin{bmatrix} B_{n+1} \\ A_{n+1} \end{bmatrix} = \begin{bmatrix} M_{11} & M_{12} \\ M_{21} & M_{22} \end{bmatrix} \begin{bmatrix} B_n \\ A_n \end{bmatrix} \qquad n = 0, 1, 2, \ldots, N-1 \tag{4.18}$$

with

$$\begin{aligned}
B_0 &= \frac{2g^2}{\omega^2}, \qquad A_0 = -\frac{2g^2}{\omega^2} - \frac{1}{4} - \delta + \frac{N}{2} \\
M_{11} &= -\frac{2g^2}{\omega^2}\left(\frac{1}{4} - \delta + \frac{N}{2}\right) \\
M_{12} &= -\frac{2g^2}{\omega^2}\left(\frac{1}{4} - \delta + n - \frac{N}{2}\right) \\
M_{21} &= \left(\frac{2g^2}{\omega^2} + \frac{5}{4} + \delta + n - \frac{N}{2}\right)\left(\frac{1}{4} - \delta + \frac{N}{2}\right) - \frac{2g^2}{\omega^2}(n+1) \\
M_{22} &= \left(\frac{2g^2}{\omega^2} + \frac{5}{4} + \delta + n - \frac{N}{2}\right)\left(\frac{1}{4} - \delta + n - \frac{N}{2}\right) - \frac{2g^2}{\omega^2}(n+1) \\
\delta &\equiv \frac{\omega_0 - \omega}{4\omega}.
\end{aligned} \tag{4.19}$$

For a given value of N, the sum $A_N + B_N$ is a polynomial of degree N in g^2, and (4.17) thus yields N solutions for g^2. The positive square roots of the positive g^2 solutions to (4.17) yield the values of the coupling for which Juddian isolated exact solutions exist, and the energies corresponding to these couplings then lie on the Nth so-called baseline, defined by

$$E_N^{\text{Baseline}} = N\omega - \frac{4g^2}{\omega}. \tag{4.20}$$

For $N = 0$, $A_0 + B_0 = -\frac{1}{4} - \delta$, which is independent of the coupling g, and (4.17) is then only satisfied in the special case $\delta = -\frac{1}{4}$, which corresponds to $\omega_0 = 0$ *i.e.* degenerate atomic levels. It is then clear from (4.20) that the Juddian solution for $N = 0$ and $\omega_0 = 0$ yields the $\omega_0 = 0$ solution (4.11) presented in Section 4.1, which is a degenerate ground–state solution analytic for all couplings. This two–fold degeneracy is a generic feature of the Juddian solutions for the Rabi Hamiltonian for all N, and indicates that these solutions always occur at points where two energy levels simultaneously cross the Nth baseline.

For $N = 0$ and $\omega_0 \neq 0$, isolated exact solutions do not exist for any value of the coupling g. In fact, at least at resonance ($\omega_0 = \omega$ or equivalently $\delta = 0$), no Juddian solutions occur for either the ground or first excited states of the Rabi system for any value of the coupling [Re82]. For $N > 0$, however, isolated analytic solutions corresponding to higher lying states of the Rabi Hamiltonian may be found at particular values of g, and these Juddian solutions then provide a useful benchmark against which approximate results may be checked.

Although in this thesis we focus mainly on the coupled cluster method, it is of interest for purposes of comparison to analyze the Rabi system using other many–body techniques. In particular, we consider here techniques which yield quasi–exact numerical results. The configuration–interaction (CI) method (also known as the Rayleigh-Ritz method or simply diagonalization), is generally regarded as such a method, and entails the diagonalization of a Hamiltonian in a subspace of the full many–body Hilbert space. For any

given range of values of the coupling g, care must be taken to ensure that the dimension N of the subspace is large enough so that the calculation may be deemed to have converged at each value of g in the given interval. This typically requires $N \sim 100$, so that the diagonalization has to be done numerically. We construct a typical subspace as the span of a basis consisting of products of bosonic occupation number states and two–level atomic states. Since the Rabi Hamiltonian (4.1) conserves the parity (4.2), the matrix representation of (4.1) blocks into even and odd parity sectors, simplifying the numerical calculation.

It is important to note that there is no *a priori* guarantee that the CI results, even when done to arbitrarily high (finite) order N, are practically exact (see *e.g.* [Lo98], where it is demonstrated that this is not the case for the multiquantum or k–photon Rabi model). For the Rabi Hamiltonian, however, we may use the Juddian solutions to benchmark the CI results. As shown in Table 4.1, a CI diagonalization of the scaled resonant Rabi Hamiltonian in a basis of $N \geq 61$ states reproduces the known exact results for the ninth and tenth excited states at the representative Juddian point $g = g^* = 0.75824924$ to within the limits of numerical precision ($< 10^{-10}$). In Table 4.1 we also tabulate the (even–parity) ground state and (odd–parity) first excited state energies at $g = g^*$. Although there does not appear to be a formal proof of this, it is reasonable to expect that, in the same order N, the error in the lower–lying energies should be at most of the same order of magnitude as that for the higher–lying states, particularly since the lower–lying energy eigenvalues appear to converge at least as quickly with increasing N as their

higher–lying counterparts [2]. Results of similar accuracy may be obtained at other Juddian points, and we may thus assert that the CI results are for all practical purposes exact over the full coupling spectrum.

Table 4.1: *Comparison of the results of a CI diagonalization of the scaled resonant ($\omega = \omega_0 = 1$) Rabi Hamiltonian in a basis of N states with the Juddian solution occurring at $g = g^* = 0.75824924$ for which the exact energies of the ninth (E_9) and tenth (E_{10}) excited states are given by $E_9 = E_{10} = E^* = 1.70023235$. Clearly the CI method effectively reproduces the exact Juddian result for $N \geq 61$. Also shown are the CI results for the even–parity ground (E_0) and odd–parity first excited (E_1) state energies at the same coupling g^*. The converged CI results for E_0 and E_1 are clearly well separated at this value of g.*

N	$E_9^{(N)}$	$E_{10}^{(N)}$	$E_9^{(N)} - E^*$	$E_{10}^{(N)} - E^*$	$E_0^{(N)}$	$E_1^{(N)}$	$E_1^{(N)} - E_0^{(N)}$
11	5.40691445	7.30537548	3.7067×10^{0}	5.6051×10^{0}	-2.2528	-2.1830	6.9734×10^{-2}
21	2.36187405	2.36800390	6.6164×10^{-1}	6.6777×10^{-1}	-2.3361	-2.3247	1.1383×10^{-2}
31	1.70942030	1.74049648	9.1879×10^{-3}	4.0264×10^{-2}	-2.3363	-2.3255	1.0753×10^{-2}
41	1.70024476	1.70027293	1.2407×10^{-5}	4.0578×10^{-5}	-2.3363	-2.3255	1.0753×10^{-2}
51	1.70023235	1.70023236	7.9560×10^{-10}	8.5000×10^{-9}	-2.3363	-2.3255	1.0753×10^{-2}
61	1.70023235	1.70023235	8.8867×10^{-12}	9.8461×10^{-11}	-2.3363	-2.3255	1.0753×10^{-2}
101	1.70023235	1.70023235	1.8695×10^{-11}	8.6098×10^{-11}	-2.3363	-2.3255	1.0753×10^{-2}

[2] Although theorems such as those on interleaving eigenvalues may in certain cases be used to bracket the exact eigenvalues, we have not been able to find any useful theorems relating the rate of convergence (with increasing N) of the higher–lying eigenvalues to that of the lowest eigenvalues in the literature.

4.2 Physical characteristics of the Rabi ground state

Systems similar to the Rabi Hamiltonian are known to exhibit interesting ground–state behaviour. A case in point is the polaron, consisting of an electron interacting with the phononic lattice field in a solid [Mah]. It is well known that there is a crossover from the so–called large polaron regime, where the electron is essentially free to roam the solid (and the Fröhlich Hamiltonian, which treats the ionic background as a continuum, applies), to the small polaron regime, where the discrete nature of the lattice manifests itself and the electron is to a greater or lesser degree localized to a particular atomic site. The crossover from large to small polaron behaviour as the electron–phonon coupling is increased does not constitute a phase transition, but it does signify a drastic change in the character of the polaron ground state in a reasonably well–defined coupling regime. In fact, an application of time–independent (Rayleigh–Schrödinger) perturbation theory (TIPT) to the Fröhlich Hamiltonian yields an infinite effective mass for the electron at a particular value of the coupling (see [Mah] and references therein), an obviously erroneous result which may however be used to identify the crossover regime. Similar crossover behaviour is also observed in the study of a quantum particle tunneling between two wells in the presence of a phonon bath (see [Lo95] and references therein). In this system, which is closely analogous to the Rabi Hamiltonian and which may also be used as a model of the two–site polaron, there is competition between the localization inherent in the interaction with the phonons, and the delocalization inherent in

the tunneling. Again, although several variational studies find evidence for a sharp (discontinuous) transition, the localization–delocalization crossover which occurs for intermediate coupling between the particle and the phonons does not consitute a true phase transition, but simply a change in character in the ground state of the system.

It is thus not surprising to find that a similar crossover regime exists for the quantum optical system described by the Rabi Hamiltonian. Using the (essentially exact) CI results for the resonant Rabi ground–state wave function, we have also determined the expectation value $\langle \sigma^z \rangle$, which indicates to what extent the atom may be regarded as being in its upper or lower state, as well as the fluctuation $\Delta\sigma^z = \sqrt{1 - \langle \sigma^z \rangle^2}$, as a function of the coupling g. The results, which are shown in Figure 4.1, indicate that there is a marked change in the physical character of the ground–state wave function in the region where $g \sim 0.6$. Below this transitional region, the atom is predominantly in its lower state. Above the transitional region, the atom is essentially in an equal superposition of the upper and lower states. The change in character in the ground state also manifests itself in $\langle n \rangle$, the average number of photons in the field in the Rabi ground state, as well as in the fluctuation Δn in the photon number, as a function of the coupling g. Again using the CI result for the Rabi ground–state wave function at resonance, we find that $\langle n \rangle \approx \Delta n \approx 1$ at $g \sim 0.6$, which defines the same transitional region as before.

The change in character in the Rabi ground state, although marked, is not discontinuous, and there is thus no evidence for a phase transition. Note that

the Rabi system has an infinite number of degrees of freedom (the number of bosons can be infinite), and that, unlike a finite system, it could in principle display a true phase transition. If such a phase transition were present, the ground and first excited states would become degenerate at the critical coupling for the transition. The absence of such a transition is thus also substantiated by the CI results for the ground and first excited state energies E_0 and E_1, which are well separated in the transitional region, even (see

Figure 4.1: *The expectation value $\langle\sigma^z\rangle$ (solid line) and the fluctuation $\Delta\sigma^z$ (thick solid line) in the ground state of the scaled resonant ($\omega = \omega_0 = 1$) Rabi Hamiltonian, as a function of the coupling g, as determined via a CI diagonalization in a basis of 101 even–parity states.*

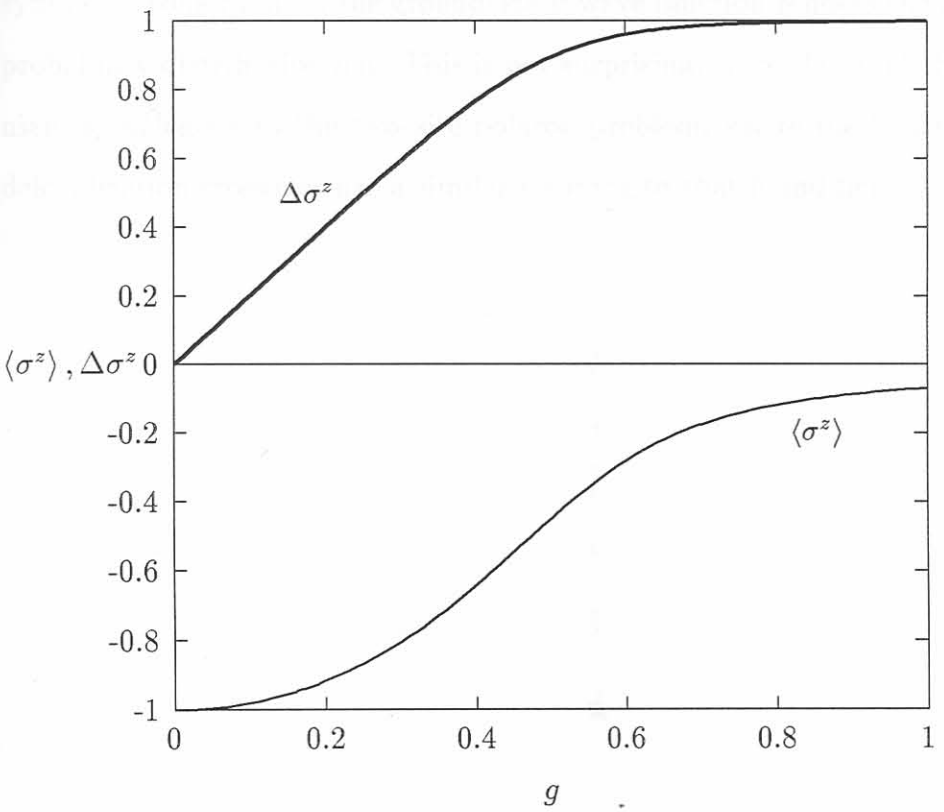

Table 4.1) at the Juddian point $g = g^* = 0.75824924$ located well above this region. Even in the limit $\omega_0 = 0$ where the (analytic) ground state is doubly degenerate for all couplings and there is definitely no phase transition, this continuous yet marked character change still occurs in the even–parity ground state $|\Psi_+\rangle$ (see Figure 4.3).

For the Fröhlich polaron problem, the large–to–small polaron crossover is accompanied by a localization of the electronic wave packet in configuration space. No such localization occurs in the angular wave packet associated with the angle variable conjugate to σ^z [Ca68, Za69, Pei], since the even–parity symmetry constraint on the ground–state wave function renders the angular probability distribution flat. This is not surprising, since the Rabi Hamiltonian is analogous to the two–site polaron problem, where the localization–delocalization crossover has a similar meaning to that found here.

4.3 Approximate many–body approaches to the Rabi Hamiltonian

Historically, the non–rotating terms included in the Rabi Hamiltonian were considered to act merely as sources of small frequency shifts, the so–called Bloch–Siegert shifts, with respect to the Jaynes–Cummings spectrum [Bl40] (see also [Mi91, Sh93] and references therein). As discussed in Section 4.1, however, there has been renewed interest in the full Rabi Hamiltonian (4.1), and recent many–body analyses of the Hamiltonian include, amongst others, a weak–coupling time–independent perturbative expansion in g [Ph89, Qi98], a first–order strong coupling perturbative expansion in ω_0 [Gr84b], a calculation based on a variational coherent state [Qi98], and a path–integral approach applied in the weak coupling regime [Za88]. Also, numerically exact (though not analytic) results for the Rabi system have recently been obtained via the operator method [Fe96], via a power series solution [Qi98], and via a combination of unitary transformations and numerical diagonalization [Lo96].

4.3.1 Time–independent perturbation theory

Consider first the application of time–independent (Rayleigh–Schrödinger) perturbation theory to the Rabi Hamiltonian (see also [Ph89, Qi98]). We write

$$H_{\text{Rabi}} = H^{(0)}_{\text{Rabi}} + gH'_{\text{Rabi}} \tag{4.21}$$

where

$$\begin{aligned} H^{(0)}_{\text{Rabi}} &\equiv \frac{1}{2}\omega_0\sigma^z + \omega b^\dagger b \,, \\ H'_{\text{Rabi}} &\equiv \left(b^\dagger + b\right)\left(\sigma^+ + \sigma^-\right) \,. \end{aligned} \tag{4.22}$$

We restrict the perturbative calculation to the even–parity sector, and only consider $\omega_0 \neq 0$. Since the spectrum of $H^{(0)}_{\text{Rabi}}$, the "noninteracting" ($g = 0$) Rabi Hamiltonian is simply determined as

$$\begin{aligned} H^{(0)}_{\text{Rabi}}|\Psi^{(0)}_m\rangle &= E^{(0)}_m|\Psi^{(0)}_m\rangle \qquad m = 0, 1, 2, \ldots \\ |\Psi^{(0)}_m\rangle &= \begin{cases} |m\rangle|\downarrow\rangle & m \text{ even} \\ |m\rangle|\uparrow\rangle & m \text{ odd} \end{cases} \\ E^{(0)}_m &= m\omega - \frac{(-1)^m}{2}\omega_0 \,, \end{aligned} \tag{4.23}$$

and since furthermore the ground state of $H^{(0)}_{\text{Rabi}}$ is nondegenerate for $\omega_0 \neq 0$, a perturbative ground–state expansion in powers of the coupling g is feasible and in principle straightforward. To Nth order, we expand the true ground–state wave function $|\Psi_0\rangle$ and energy E_0 as

$$\begin{aligned} |\Psi_0\rangle &= |\Psi^{(0)}_0\rangle + \sum_{i=1}^{N} g^i|\Psi^{(i)}_0\rangle = |0\rangle|\downarrow\rangle + \sum_{i=1}^{N} g^i|\Psi^{(i)}_0\rangle \\ E_0 &= E^{(0)}_0 + \sum_{i=1}^{N} g^i E^{(i)}_0 = -\frac{1}{2}\omega_0 + \sum_{i=1}^{N} g^i E^{(i)}_0 \,. \end{aligned} \tag{4.24}$$

We express the ith order correction $|\Psi^{(i)}_0\rangle$ to the ground–state wave function in the basis consisting of the eigenstates of $H^{(0)}_{\text{Rabi}}$ via

$$|\Psi^{(i)}_0\rangle = \sum_{m=1}^{M} c^{(i)}_m|\Psi^{(0)}_m\rangle \,, \qquad i = 1, 2, \ldots, N \,, \tag{4.25}$$

where M is a cutoff introduced for computational purposes. The neglect of the $m = 0$ term in (4.25) simply results in an overall rescaling of the

perturbative ground–state wave function [Mer]. Upon substituting (4.24) and (4.25) into the Schrödinger equation $H|\Psi_0\rangle = E_0|\Psi_0\rangle$, and comparing terms of equal order in g, we obtain the equations

$$\begin{aligned}\left(E_m^{(0)} - E_0^{(0)}\right) c_m^{(i)} &= 2\sum_{j=2}^{i-1} c_1^{(j-1)} c_m^{(i-j)} - 2\sqrt{m+1}\, c_{m+1}^{(i-1)} - 2\sqrt{m}\, c_{m-1}^{(i-1)} \\ & \qquad m = 1, 2, \ldots, M\,, \qquad i = 1, 2, \ldots, N \\ E_0^{(i)} &= 2\, c_1^{(i-1)}\,, \qquad\qquad i = 1, 2, \ldots, N\,, \end{aligned} \tag{4.26}$$

which are to be solved for the required unknowns $\{c_m^{(i)}\}$ and $\{E_0^{(i)}\}$. These equations must be solved for M large enough so that the results are effectively independent of M, *i.e.* so that we may safely neglect $\{c_m^{(i)}; i = 1, 2, \ldots, N\}$ for all $m > M$. This calculation, which we shall refer to as weak–coupling perturbation theory, may be done analytically to arbitrary finite order using algebraic manipulation packages such as *Mathematica* [Mat], and the results at resonance are shown in Figure 4.2. Since the weak–coupling Rayleigh-Schrödinger perturbation series for the ground–state energy, which at resonance ($\omega = \omega_0 = 1$) assumes the form

$$E_0^{\text{Weak}} = -\frac{1}{2} - 2\,g^2 - 2\,g^4 - 2\,g^6 + 6\,g^{10} + \frac{41}{3}\,g^{12} + \frac{113}{18}\,g^{14} + \ldots\,, \tag{4.27}$$

does not appear to follow a discernably regular pattern, we have not been able to analytically determine the radius of convergence of this series. It is apparent from Figure 4.2, however, that the perturbative approach breaks down at $g \approx 0.6$, which defines the same transitional region as described in Section 4.2, and further highlights the analogy between the Rabi system and the polaron problem, where a similar breakdown in TIPT occurs.

Since the spectrum of the Rabi Hamiltonian in the limit $\omega_0 = 0$ is known [Gr84b], it is in principle also possible to analyze the Hamiltonian via strong–

Figure 4.2: *The ground–state energy E_0 of the scaled resonant ($\omega = \omega_0 = 1$) Rabi Hamiltonian as a function of the coupling g as determined via 12th, 20th and 50th order weak–coupling TIPT (solid lines), and via first order strong–coupling TIPT (thin solid line), compared to results obtained via a CI diagonalization in a basis of 101 even–parity states (thick solid line).*

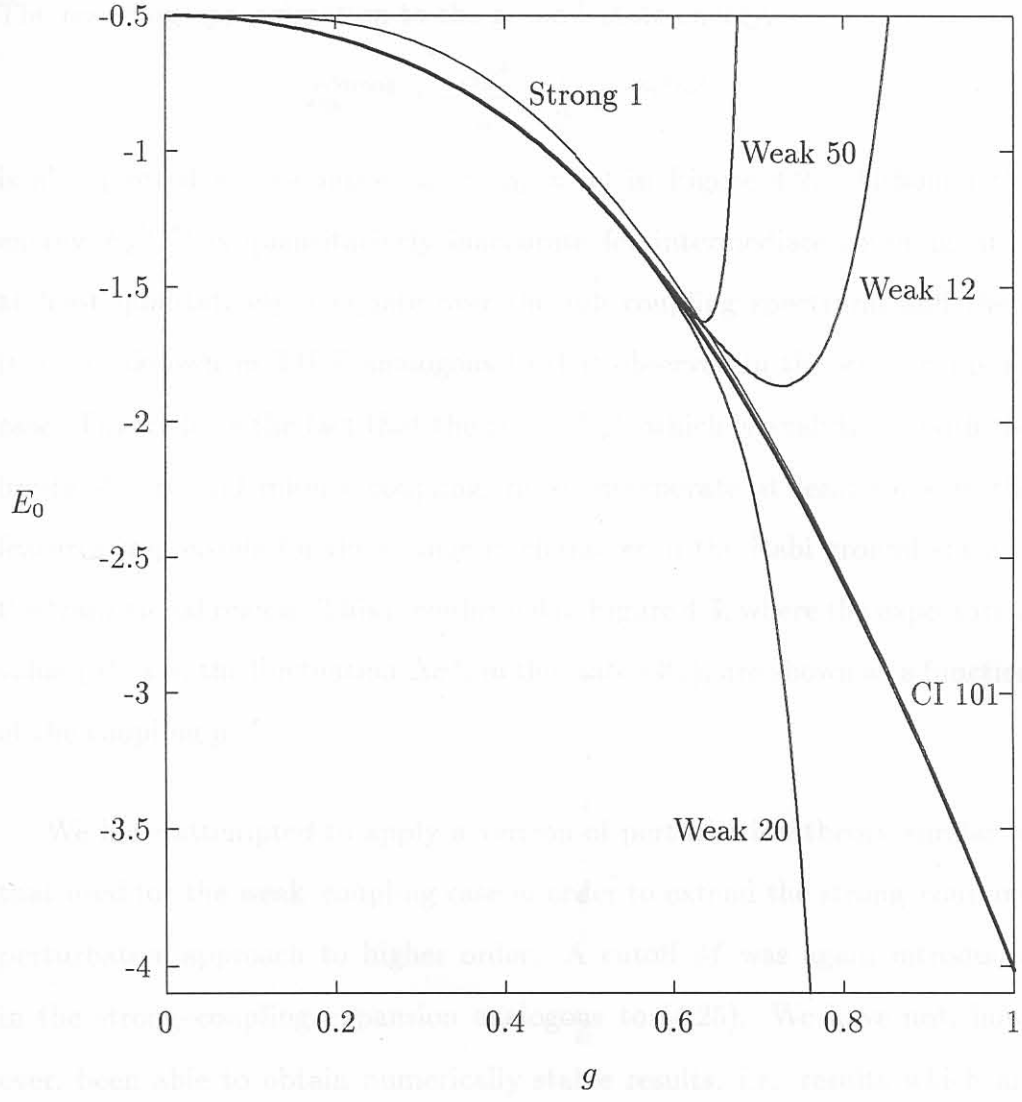

coupling perturbation theory. This involves a ground–state expansion in powers of ω_0 (see comment just before equation (4.11). The first order strong–coupling perturbative correction (which multiplies ω_0) to the $\omega_0 = 0$ ground–state energy $E_0^{(0)} = -4g^2/\omega$ is given by

$$E_0^{(1)} = \langle \Psi_+ | \frac{1}{2}\sigma^z | \Psi_+ \rangle = -\frac{1}{2} e^{-8g^2/\omega^2} , \tag{4.28}$$

where $|\Psi_+\rangle$ is the positive–parity $\omega_0 = 0$ ground state introduced in (4.16). The resulting approximation to the ground–state energy,

$$E_0^{\text{Strong}} = -\frac{4g^2}{\omega} - \frac{1}{2}\omega_0 e^{-8g^2/\omega^2} , \tag{4.29}$$

is also plotted at resonance ($\omega = \omega_0 = 1$) in Figure 4.2. Although the energy E_0^{Strong} is quantitatively inaccurate for intermediate coupling, it is at least qualitatively adequate over the full coupling spectrum, and there is no breakdown in TIPT analogous to that observed in the weak–coupling case. This reflects the fact that the state $|\Psi_+\rangle$, which is analytic in both the limits of zero and infinite coupling, must incorporate at least some of the features responsible for the change in character in the Rabi ground state in the transitional region. This is confirmed in Figure 4.3, where the expectation value $\langle \sigma^z \rangle$ and the fluctuation $\Delta\sigma^z$, in the state $|\Psi_+\rangle$, are shown as a function of the coupling g.

We have attempted to apply a version of perturbation theory similar to that used for the weak–coupling case in order to extend the strong–coupling perturbative approach to higher order. A cutoff M was again introduced in the strong–coupling expansion analogous to (4.25). We have not, however, been able to obtain numerically stable results, *i.e.* results which are effectively independent of the cutoff M, using this approach.

Figure 4.3: *The expectation value* $\langle\sigma^z\rangle$ *(solid line) and the fluctuation* $\Delta\sigma^z$ *(thick solid line) in the even–parity* $\omega_0 = 0$ *ground state* $|\Psi_+\rangle$ *of the scaled resonant* $(\omega = \omega_0 = 1)$ *Rabi Hamiltonian, as a function of the coupling* g*, compared to the same quantities (dotted lines) determined via a CI diagonalization in a basis of 101 even–parity states.*

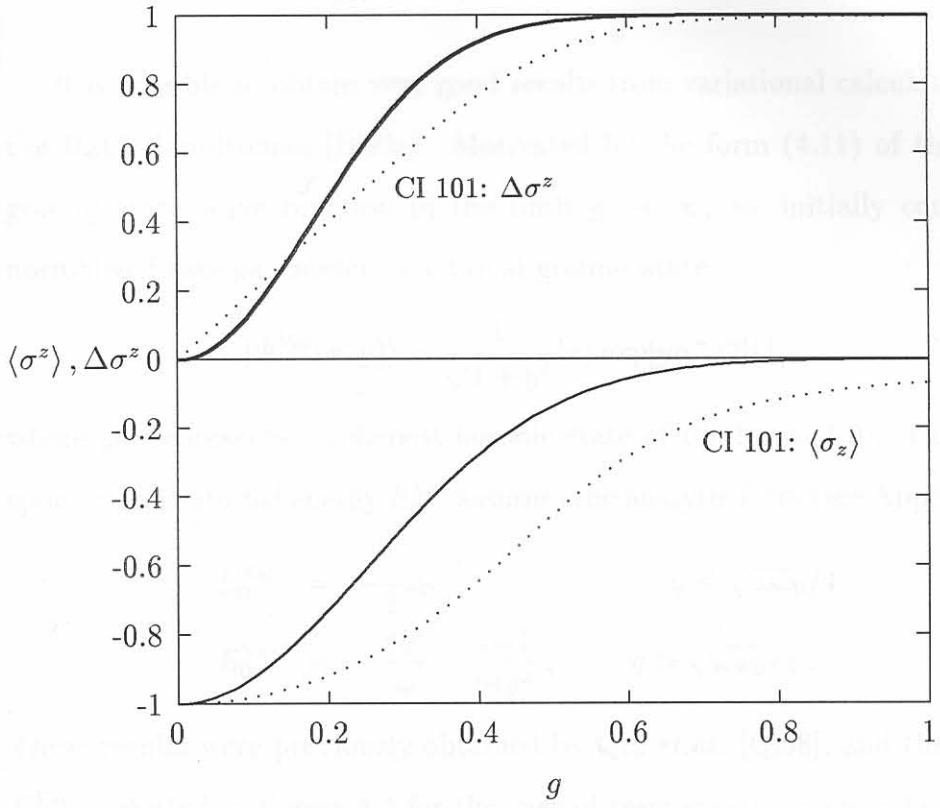

4.3.2 Variational results for the Rabi Hamiltonian

The variational method is a commonly used approach to simple many–body Hamiltonians when a computationally inexpensive estimate of the ground–state energy of the system is required. The basis of the method is a postulated ansatz for the many–body wave function, containing parameters whose values

are determined by minimizing the expectation value $\langle H \rangle$ of the Hamiltonian in the trial state. This minimal expectation value (*i.e.* $\langle H \rangle$ evaluated at the optimal values of the variational parameters) yields an estimate of the ground–state energy. A considerable advantage of the variational method is that the approximate energy thus obtained provides an upper bound for the exact ground–state energy for any choice of the trial wave function.

It is possible to obtain very good results from variational calculations for the Rabi Hamiltonian [Bi99a]. Motivated by the form (4.11) of the exact ground–state wave function in the limit $g \to \infty$, we initially consider a normalized two–parameter variational ground state

$$|\Psi^{\mathrm{Var}}(x,y)\rangle = \frac{1}{\sqrt{1+y^2}}|x\rangle \exp[y\sigma^+/2]|\downarrow\rangle \ , \tag{4.30}$$

where $|x\rangle$ represents a coherent bosonic state of the form (4.9). The corresponding variational energy E_0^{Var} assumes the analytic form (see Appendix C)

$$\begin{aligned} E_0^{\mathrm{Var}} &= -\frac{1}{2}\omega_0 \ , & g \leq \sqrt{\omega\omega_0}/4 \\ E_0^{\mathrm{Var}} &= -\frac{4g^2}{\omega} - \frac{\omega\omega_0^2}{64g^2} \ , & g > \sqrt{\omega\omega_0}/4 \ . \end{aligned} \tag{4.31}$$

These results were previously obtained by Qin *et.al.* [Qi98], and the energy E_0^{Var} is plotted in Figure 4.4 for the case of resonance ($\omega = \omega_0 = 1$).

It is clear that, for a coherent variational state of the form (4.30), the variational ground–state energy may at best be regarded as qualitatively acceptable. Furthermore, although E_0^{Var} is both continuous and differentiable (smooth) at the crossover point $g = \sqrt{\omega\omega_0}/4$ between the two branches of the variational solution, there is a discontinuity in the second derivative $d^2E_0^{\mathrm{Var}}/dg^2$ at this point. By contrast, a numerical differentiation of the CI

(large scale diagonalization) result for the Rabi ground–state energy yields smooth results for both the first and second order derivatives of E_0 with respect to g. We are thus led to seek a variational trial state better capable of following the character change in the Rabi ground state.

Figure 4.4: *The ground–state energy E_0 of the scaled resonant ($\omega = \omega_0 = 1$) Rabi Hamiltonian as a function of the coupling g as determined via a variational calculation based on the mixed parity two–parameter coherent state (4.30) (thin solid line), as well as via an even–parity projection after variation (PAV) based on the same state (dotted solid line, see (4.35)), compared to results obtained via a CI diagonalization in a basis of 101 even–parity states (thick solid line).*

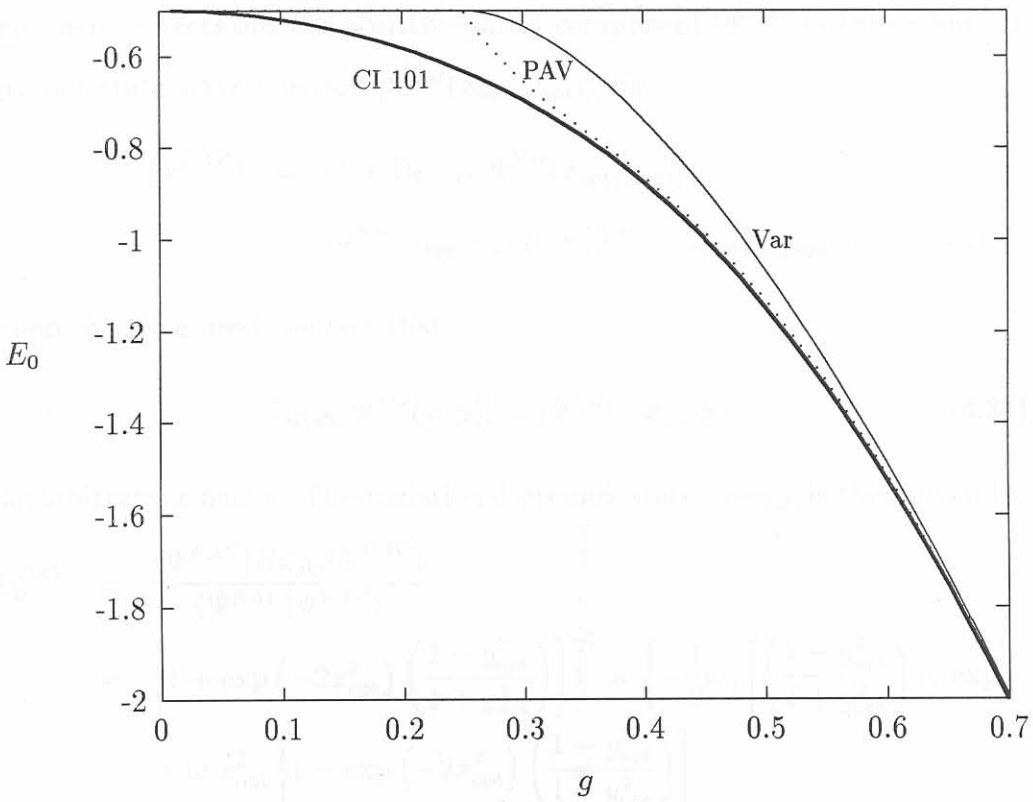

The important omission from the variational ansatz (4.30) is that the parity symmetry $\Pi_{\rm Rabi}$ of the Hamiltonian has not been taken into account. We know from the CI (diagonalization) results that the exact ground state of the Rabi Hamiltonian is of even parity, and it is clear that the state

$$\begin{aligned} |\Psi^{\rm Var}(x,y)\rangle &= \frac{1}{\sqrt{1+y^2}}|x\rangle \exp[y\sigma^+/2]|\downarrow\rangle \\ &= \frac{1}{\sqrt{1+y^2}}\, e^{-x^2/2} \sum_{n=0}^{\infty} \frac{x^n}{\sqrt{n!}}\, |n\rangle \, \{|\downarrow\rangle + y|\uparrow\rangle\} \end{aligned} \tag{4.32}$$

does not have good $\Pi_{\rm Rabi}$ parity. There are two possibilities for incorporating the correct parity symmetry into the variational calculation. In the approach known as projection after variation (PAV), the optimal values $x_{\rm opt}$ and $y_{\rm opt}$ of the variational parameters x and y in (4.30) are determined as before, and one then projects out the positive–parity component $|\Psi^{PAV}\rangle$ of the resulting ground–state wave function $|\Psi^{\rm Var}(x_{\rm opt}, y_{\rm opt})\rangle$ via

$$\begin{aligned} |\Psi^{PAV}\rangle &= (1+\Pi_{\rm Rabi})\,|\Psi^{\rm Var}(x_{\rm opt}, y_{\rm opt})\rangle \\ &= |\Psi^{\rm Var}(x_{\rm opt}, y_{\rm opt})\rangle + |\Psi^{\rm Var}(-x_{\rm opt}, -y_{\rm opt})\rangle\,, \end{aligned} \tag{4.33}$$

where we have used the fact that

$$\Pi_{\rm Rabi}|\Psi^{\rm Var}(x,y)\rangle = |\Psi^{\rm Var}(-x,-y)\rangle \tag{4.34}$$

for arbitrary x and y. The variational ground–state energy is then given by

$$\begin{aligned} E_0^{PAV} &= \frac{\langle\Psi^{PAV}|H_{\rm Rabi}|\Psi^{PAV}\rangle}{\langle\Psi^{PAV}|\Psi^{PAV}\rangle} \\ &= \left[1+\exp\left(-2x_{\rm opt}^2\right)\left(\frac{1-y_{\rm opt}^2}{1+y_{\rm opt}^2}\right)\right]^{-1} \times \left\{-\frac{1}{2}\omega_0\left[\left(\frac{1-y_{\rm opt}^2}{1+y_{\rm opt}^2}\right)+\exp\left(-2x_{\rm opt}^2\right)\right]\right. \\ &\quad + \omega\, x_{\rm opt}^2\left[1-\exp\left(-2x_{\rm opt}^2\right)\left(\frac{1-y_{\rm opt}^2}{1+y_{\rm opt}^2}\right)\right] \\ &\quad \left. + 8g\left(\frac{y_{\rm opt}x_{\rm opt}}{1+y_{\rm opt}^2}\right)\right\}\,. \end{aligned} \tag{4.35}$$

The PAV ground–state energy results are also shown in Figure 4.4, and it is clear that, although there is considerable improvement on the mixed–parity variational results for large coupling, the PAV approach still fails at intermediate coupling where the mixed parity variational results are poor. It is also apparent from Figure 4.4 that the derivative dE_0^{PAV}/dg (rather than $d^2E_0^{PAV}/dg^2$) is already discontinuous at the crossover point $g = \sqrt{\omega\omega_0}/4$, so that the PAV approach actually accentuates the spurious discontinuity in the Rabi ground state.

To include the parity in a self–consistent manner, we consider projection before variation (PBV). We construct (as yet unnormalized) states of good parity from the mixed–parity two–parameter state $|\Psi^{\rm Var}(x,y)\rangle$ (here x and y are still free variational parameters) by projection:

$$\begin{aligned} |\Psi_\pm^{\rm PBV2}(x,y)\rangle &\propto (1 \pm \Pi_{\rm Rabi})\,|\Psi^{\rm Var}(x,y)\rangle \\ &= |\Psi^{\rm Var}(x,y)\rangle \pm |\Psi^{\rm Var}(-x,-y)\rangle \\ &\propto \{|x\rangle \pm |-x\rangle\}\,|\downarrow\rangle \;+\; y\;\{|x\rangle \mp |-x\rangle\}\,|\uparrow\rangle \\ &= |x\rangle_\pm|\downarrow\rangle + y\,|x\rangle_\mp|\uparrow\rangle\,, \end{aligned} \tag{4.36}$$

where

$$\begin{aligned} |x\rangle_+ &\equiv |x\rangle + |-x\rangle = 2\,e^{-x^2/2}\sum_{n=0}^{\infty}\frac{x^{2n}}{\sqrt{(2n)!}}|2n\rangle \\ |x\rangle_- &\equiv |x\rangle - |-x\rangle = 2\,e^{-x^2/2}\sum_{n=0}^{\infty}\frac{x^{2n+1}}{\sqrt{(2n+1)!}}|2n+1\rangle\,, \end{aligned} \tag{4.37}$$

and the upper (lower) sign in (4.36) thus clearly denotes a state with positive (negative) parity. Thus we obtain, besides the positive–parity state which approximates the Rabi ground state, also a negative–parity ansatz for the

first excited state. For numerical reasons, it turns out to be more convenient to normalize the states $|x\rangle_{\pm}|\downarrow\rangle$ and $|x\rangle_{\mp}|\uparrow\rangle$ individually before constructing the combination, and we therefore consider the two–parameter variational states [Bi99a]

$$|\Psi_{\pm}^{\mathrm{PBV2}}(x,v)\rangle = A_v\left(A_{\pm}|x\rangle_{\pm}|\downarrow\rangle + vA_{\mp}|x\rangle_{\mp}|\uparrow\rangle\right) , \tag{4.38}$$

where as before the upper (lower) sign refers to a state of even (odd) Π_{Rabi} parity, and

$$\begin{aligned} A_v &= \left(1+v^2\right)^{-1/2} , \\ A_{\pm} &= \left(2\left[1 \pm e^{-2x^2}\right]\right)^{-1/2} . \end{aligned} \tag{4.39}$$

The minimization of the expectation value

$$\langle H_{\mathrm{Rabi}}\rangle_{\pm}^{\mathrm{PBV2}}(x,v) \equiv \langle\Psi_{\pm}^{\mathrm{PBV2}}(x,v)|H_{\mathrm{Rabi}}|\Psi_{\pm}^{\mathrm{PBV2}}(x,v)\rangle \tag{4.40}$$

with respect to x and v yields two equations for the optimal values x_{opt} and v_{opt} of the variational parameters (see Appendix C). For both the positive– and negative–parity cases, the equation for v_{opt} is analytically soluble, so that the variational (PBV) approach based on the two–parameter state (4.38) only requires the numerical solution of one non–linear equation in the single unknown x_{opt}. We will denote the positive–parity variational ground–state energy thus obtained by E_0^{PBV2}, and the corresponding negative–parity first excited state energy by E_1^{PBV2}.

The inclusion of the correct parity symmetry in the variational ansatz yields a dramatic quantitative improvement in the variational estimate for the ground–state energy of the Rabi system. On the scale of our graphs, the

results for E_0^{PBV2} are indistinguishable from the diagonalization results over the full coupling spectrum, and in Table 4.2 we therefore tabulate E_0^{PBV2}, together with the optimal values x_{opt} and v_{opt}, as a function of g for a range of frequencies. For comparison, we also tabulate the converged CI results

Table 4.2: *Comparison of the ground-state energy of the Rabi Hamiltonian obtained from a PBV calculation based on the even-parity two-parameter ansatz (4.38), E_0^{PBV2}, with the results of a CI diagonalization in a basis of 101 even-parity states, E_0^{CI}. Also shown are the percentage error $\left|E_0^{\mathrm{PBV2}} - E_0^{\mathrm{CI}}\right| / E_0^{\mathrm{CI}} \times 100$, and the values of the variational parameters x_{opt} and v_{opt} at the stationary point of the energy.*

ω_0	ω	g	E_0^{PBV2}	E_0^{CI}	% Error	x_{opt}	v_{opt}
1.0	1.0	0.05	-5.05012×10^{-1}	-5.05013×10^{-1}	2×10^{-4}	0.071	-0.050
		0.1	-5.20201×10^{-1}	-5.20202×10^{-1}	2×10^{-4}	0.142	-0.101
		0.2	-5.83285×10^{-1}	-5.83327×10^{-1}	7×10^{-3}	0.291	-0.208
		0.5	-1.14211	-1.14795	5×10^{-1}	0.859	-0.626
		1.0	-4.01580	-4.01693	3×10^{-2}	1.995	-0.939
		2.0	-1.60039×10^{1}	-1.60040×10^{1}	6×10^{-4}	4.000	-0.984
		5.0	-1.00001×10^{2}	-1.00001×10^{2}	$< 1\times10^{-4}$	10.000	-0.998
1.0	2.0	0.05	-5.03334×10^{-1}	-5.03335×10^{-1}	2×10^{-4}	0.041	-0.033
		0.1	-5.13362×10^{-1}	-5.13363×10^{-1}	2×10^{-4}	0.082	-0.067
		0.2	-5.53807×10^{-1}	-5.53809×10^{-1}	4×10^{-4}	0.164	-0.135
		0.5	-8.51754×10^{-1}	-8.51992×10^{-1}	3×10^{-2}	0.424	-0.416
		1.0	-2.10416	-2.10825	2×10^{-1}	0.938	-0.747
		2.0	-8.00798	-8.00855	7×10^{-3}	1.999	-0.969
		5.0	-5.00012×10^{1}	-5.00013×10^{1}	2×10^{-4}	5.000	-0.995
2.0	1.0	0.05	-1.00334	-1.00334	$< 1\times10^{-4}$	0.058	-0.033
		0.1	-1.01345	-1.01345	$< 1\times10^{-4}$	0.116	-0.067
		0.2	-1.05530	-1.05533	3×10^{-3}	0.237	-0.138
		0.5	-1.42799	-1.43655	6×10^{-1}	0.699	-0.430
		1.0	-4.06288	-4.06746	1×10^{-1}	1.983	-0.882
		2.0	-1.60156×10^{1}	-1.60159×10^{1}	2×10^{-3}	3.998	-0.969
		5.0	-1.00002×10^{2}	-1.00003×10^{2}	1×10^{-3}	10.000	-0.995

for the ground–state energy, as well as the percentage error in E_0^{PBV2} as compared to the CI results. The percentage error is less than 1 % over the full range of couplings and frequencies. Note that the parameters x_{opt} and v_{opt} evolve smoothly from their $g = 0$ values of 0 to their large–g values of $2g/\omega$ and -1, respectively, where it is easily seen that they correspond to a positive–parity solution of the form (4.16).

Table 4.3 contains the analogous results for a two–parameter PBV calculation of the (negative–parity) first excited state energy. The results are good — the large percentage error in regions where the first excited state energy is close to zero is artificial, since the absolute error is small in all cases. The first excited state results are however not in general at the same level of accuracy as those for the ground state, particularly for small coupling in the sub–resonant case ($\omega_0 = 2\omega$). This may be attributed to the absence of two–boson correlations in the variational ansatz (4.38). For ω_0 much larger than ω, it would be necessary to determine which n–boson correlations need to be included in the variational ansatz. For resonance and supra–resonance ($\omega_0 \leq \omega$), however, the calculation presented here is acceptable.

Although variational calculations are useful in determining energies, particularly due to the upper–bound nature of their results, there is no guarantee that the variational wave function itself is accurate. A failure of the wave function is usually revealed in the calculation of expectation values of quantities other than the Hamiltonian. To examine the quality of the (positive–parity) ground–state ansatz (4.38), we have therefore calculated the expectation values $\langle \sigma^z \rangle^{\mathrm{PBV2}}$ and $\langle b^\dagger b \rangle^{\mathrm{PBV2}}$ in this state. Explicit expres-

sions for these quantities are given in Appendix C. In Figure 4.5, the results for $\langle\sigma^z\rangle^{\mathrm{PBV2}}$ at resonance ($\omega = \omega_0 = 1$) are compared to results obtained via numerical diagonalization, as well as results based on the mixed–parity variational ansatz (4.30). The dramatic improvement obtained by the parity

Table 4.3: *Comparison of the first excited state energy of the Rabi Hamiltonian obtained from a PBV calculation based on the odd–parity two–parameter ansatz (4.38),* E_1^{PBV2}*, with the results of a CI diagonalization in a basis of 101 odd–parity states,* E_1^{CI}*. Also shown are the percentage error* $\left|E_1^{\mathrm{PBV2}} - E_1^{\mathrm{CI}}\right| / E_1^{\mathrm{CI}} \times 100$*, and the values of the variational parameters* x_{opt} *and* v_{opt} *at the stationary point of the energy.*

ω_0	ω	g	E_1^{PBV2}	E_1^{CI}	% Error	x_{opt}	v_{opt}
1.0	1.0	0.05	3.96137×10^{-1}	3.95102×10^{-1}	3×10^{-1}	0.279	-0.982
		0.1	2.84083×10^{-1}	2.80666×10^{-1}	1.2	0.401	-0.964
		0.2	3.24806×10^{-2}	2.33675×10^{-2}	40	0.590	-0.932
		0.5	-9.98782×10^{-1}	-1.01018	1.1	1.067	-0.885
		1.0	-4.01545	-4.01658	3×10^{-2}	1.997	-0.940
		2.0	-1.60039×10^{1}	-1.60040×10^{1}	6×10^{-4}	4.000	-0.984
		5.0	-1.00001×10^{2}	-1.00001×10^{2}	$< 1\times10^{-4}$	10.000	-0.998
1.0	2.0	0.05	4.90049×10^{-1}	4.90049×10^{-1}	$< 1\times10^{-4}$	0.070	-10.050
		0.1	4.60760×10^{-1}	4.60758×10^{-1}	4×10^{-4}	0.140	-5.098
		0.2	3.50617×10^{-1}	3.50542×10^{-1}	2×10^{-2}	0.270	-2.864
		0.5	-2.69004×10^{-1}	-2.71650×10^{-1}	1	0.595	-1.355
		1.0	-1.96664	-1.97218	3×10^{-1}	1.042	-1.000
		2.0	-8.00764	-8.00821	7×10^{-3}	1.999	-0.970
		5.0	-5.00013×10^{1}	-5.00013×10^{1}	$< 1\times10^{-4}$	5.000	-0.995
2.0	1.0	0.05	-1.01956×10^{-2}	-1.65009×10^{-2}	38	0.173	-0.102
		0.1	-4.28514×10^{-2}	-6.42075×10^{-2}	33	0.340	-0.212
		0.2	-1.87367×10^{-1}	-2.35841×10^{-1}	21	0.601	-0.419
		0.5	-1.11473	-1.15708	3.8	1.079	-0.706
		1.0	-4.06213	-4.06664	1×10^{-1}	1.986	-0.882
		2.0	-1.60156×10^{1}	-1.60159×10^{1}	2×10^{-4}	3.998	-0.969
		5.0	-1.00002×10^{2}	-1.00003×10^{2}	1×10^{-4}	10.000	-0.995

projection is clearly seen, and the good–parity variational results, like those obtained via the CI method, show no evidence for any discontinuity in the Rabi ground state. The corresponding results for $\langle b^\dagger b\rangle^{\mathrm{PBV2}}$ are shown in Figure 4.6, and here the agreement with the CI diagonalization is even better — the differences between the CI and two–parameter PBV results are not

Figure 4.5: *The ground–state expectation value of σ^z for the scaled resonant ($\omega = \omega_0 = 1$) Rabi Hamiltonian in the mixed–parity two–parameter variational state (4.30) (thick solid line denoted by Var), in the two–parameter PBV state (4.38) (solid line denoted by PBV2), and in the three–parameter PBV state (4.41) (dotted line denoted by PBV3), as a function of the coupling g, compared to results obtained via a CI diagonalization in a basis of 101 even–parity states (thin solid line).*

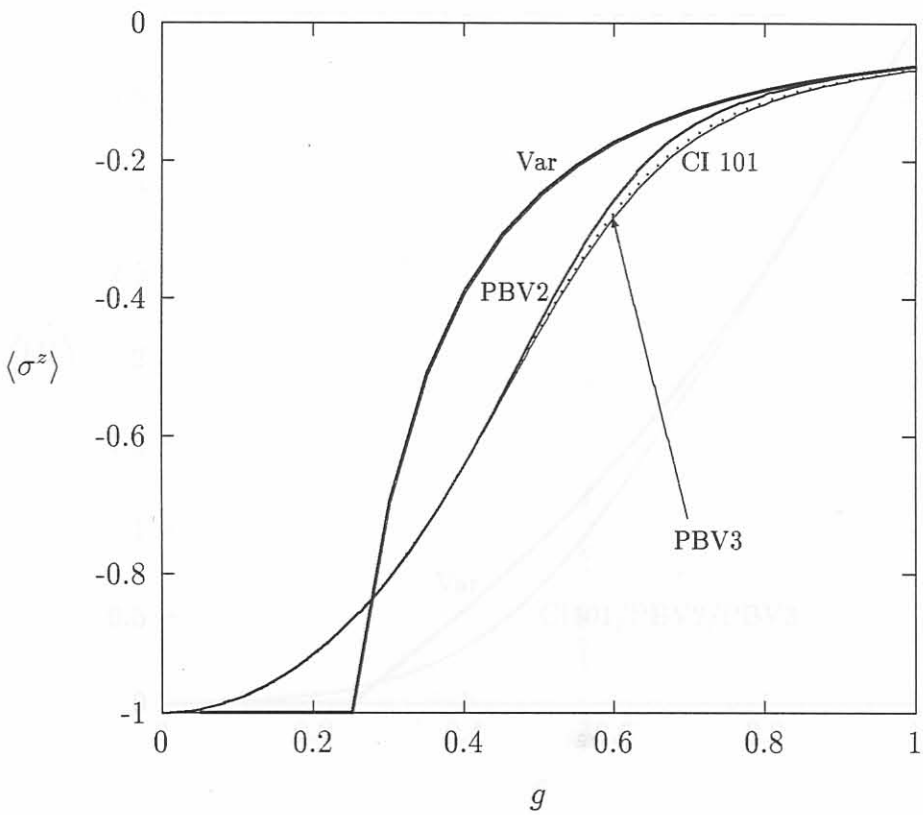

visible in the plot. Examination of the actual values shows that the variational values lie slightly below the diagonalization results for $g < 0.61$, and slightly above for larger couplings.

Figure 4.6: *The ground-state expectation value of $b^\dagger b$ for the scaled resonant ($\omega = \omega_0 = 1$) Rabi Hamiltonian in the mixed-parity two-parameter variational state (4.30) (thick solid line denoted by Var), in the two-parameter PBV state (4.38) (solid line denoted by PBV2), and in the three-parameter PBV state (4.41) (dotted line denoted by PBV3), as a function of the coupling g, compared to results obtained via a CI diagonalization in a basis of 101 even-parity states (thin solid line). On this scale, the PBV results are virtually indistinguishable from the diagonalization results.*

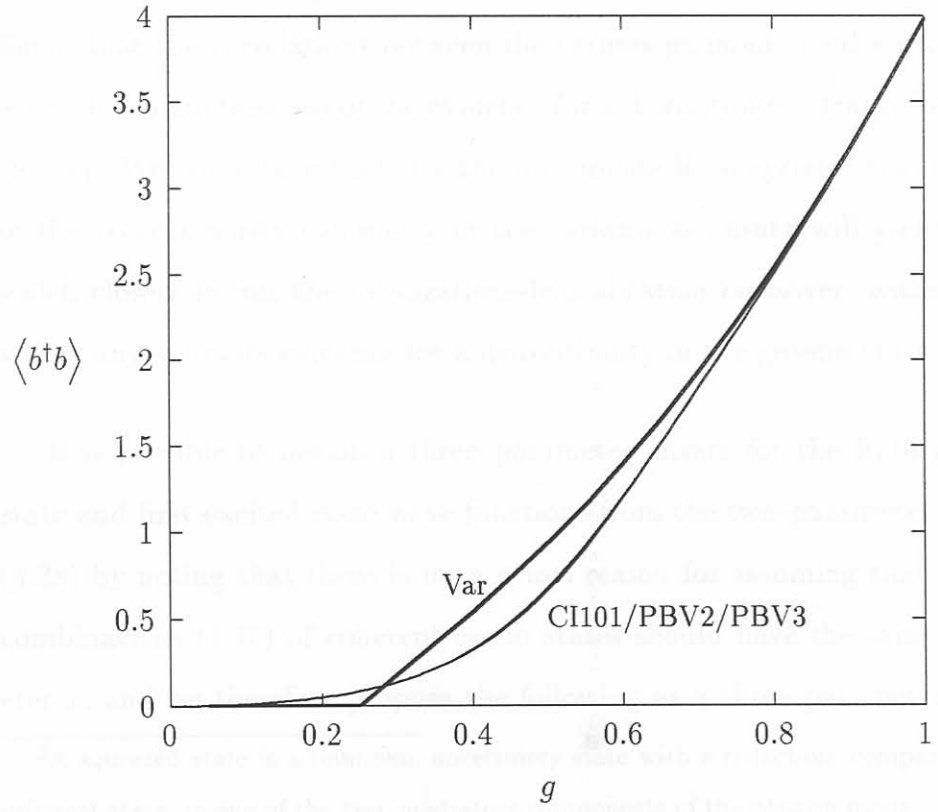

The quality of the results obtained indicates that the even–parity variational wave function (4.38) is very close to the exact ground–state wave function for the Rabi Hamiltonian, and re–emphasizes the importance of incorporating the parity symmetry in the variational calculation. In the context of a quantum tunneling system coupled to several modes of a phonon bath (see [Lo95] and references therein), variational calculations based on both a multimode coherent state and a multimode squeezed state [3] yield results which also provide evidence for a discontinuous localization–delocalization transition which turns out to be nonexistent. These results are thus analogous to the mixed–parity variational results obtained above for the Rabi Hamiltonian. Lo and Wong [Lo95] performed a variational calculation for the quantum tunneling system based on a correlated squeezed state, and found that the correlations between the various phononic modes resulted in a significant suppression of the evidence for a discontinuous transition in the system. We conjecture that, for the multimode Rabi system, the inclusion of the correct parity symmetry in the variational ansatz will yield results which closely mimic the localization–delocalization crossover, without providing any spurious evidence for a discontinuity in the ground state.

It is possible to obtain a three–parameter ansatz for the Rabi ground–state and first excited state wave functions from the two–parameter ansätze (4.38) by noting that there is no *a priori* reason for assuming that the two combinations (4.37) of coherent boson states should have the same parameter x, and we therefore propose the following as a three–parameter ansatz

[3] A squeezed state is a minimum uncertainty state with a reduction, compared to the coherent state, in one of the two quadrature components of the phonon mode.

for the Rabi Hamiltonian [Bi99a]:

$$\begin{aligned} |\Psi_{\pm}^{\mathrm{PBV3}}(x_1, x_2, v)\rangle &= A_v \left(A_{1,\pm} |x_1\rangle_{\pm} |\downarrow\rangle + v A_{2,\mp} |x_2\rangle_{\mp} |\uparrow\rangle \right) \\ &= A_v \left(A_{1,\pm} \left\{ |x_1\rangle \pm |-x_1\rangle \right\} |\downarrow\rangle \right. \\ &\quad \left. + v A_{2,\mp} \left\{ |x_2\rangle \mp |-x_2\rangle \right\} |\uparrow\rangle \right) , \end{aligned} \tag{4.41}$$

where as before the upper (lower) sign refers to a state of positive (negative) Π_{Rabi} parity, and

$$\begin{aligned} A_v &= \left[1 + v^2 \right]^{-1/2} , \\ A_{1,\pm} &= \left[2 \left(1 \pm \exp\left[-2x_1^2 \right] \right) \right]^{-1/2} , \\ A_{2,\pm} &= \left[2 \left(1 \pm \exp\left[-2x_2^2 \right] \right) \right]^{-1/2} . \end{aligned} \tag{4.42}$$

We note here that the positive–parity (negative–parity) ansatz (4.41) is clearly invariant under the replacement $x_1 \to -x_1$ ($x_2 \to -x_2$) as well as under the simultaneous replacements $x_2 \to -x_2$, $v \to -v$ ($x_1 \to -x_1$, $v \to -v$). For convenience, we consider here only the case $x_1, x_2 \geq 0$.

As shown in Appendix C, the minimization of the expectation value of H_{Rabi} in the state (4.41) again yields an analytically soluble equation for the optimal value v_{opt} of the parameter v, and it remains only to solve two coupled non-linear equations for the optimal values $x_{1,\mathrm{opt}}$ and $x_{2,\mathrm{opt}}$. Our variational results for the ground and first excited state energies for the three–parameter ansätze (4.41) are shown in Tables 4.4 and 4.5, and the percentage error relative to the diagonalization results is also plotted in Figures 4.7 and 4.8. It is clear from the values presented that we have obtained very accurate approximations for both the ground–state and first excited state energies of the Rabi Hamiltonian with very little numerical effort. The results for

the ground–state energy agree to within 0.1 % with the CI results over the full coupling and frequency spectrum, while the maximum error in the first excited state energy is of the order of 2 % (the same comments as for the two–parameter case apply here).

Table 4.4: *Comparison of the ground–state energy of the Rabi Hamiltonian obtained from a PBV calculation based on the even–parity three–parameter ansatz (4.41),* E_0^{PBV3}, *with the results of a CI diagonalization in a basis of 101 even–parity states,* E_0^{CI}. *Also shown are the percentage error* $\left|E_0^{\mathrm{PBV3}} - E_0^{\mathrm{CI}}\right| / E_0^{\mathrm{CI}} \times 100$, *and the values of the variational parameters* $x_{1,\mathrm{opt}}$, $x_{2,\mathrm{opt}}$, *and* v_{opt} *at the stationary point of the energy.*

ω_0	ω	g	E_0^{PBV3}	E_0^{CI}	% Error	$x_{1,\mathrm{opt}}$	$x_{2,\mathrm{opt}}$	v_{opt}
1.0	1.0	0.05	-5.05013×10^{-1}	-5.05013×10^{-1}	$< 1\times10^{-4}$	0.071	0.087	-0.050
		0.1	-5.20202×10^{-1}	-5.20202×10^{-1}	$< 1\times10^{-4}$	0.142	0.174	-0.101
		0.2	-5.83326×10^{-1}	-5.83327×10^{-1}	2×10^{-4}	0.292	0.351	-0.208
		0.5	-1.14676	-1.14795	1×10^{-1}	0.856	0.942	-0.618
		1.0	-4.01677	-4.01693	4×10^{-3}	1.987	2.003	-0.935
		2.0	-1.60040×10^{1}	-1.60040×10^{1}	$< 1\times10^{-4}$	3.999	4.000	-0.984
		5.0	-1.00001×10^{2}	-1.00001×10^{2}	$< 1\times10^{-4}$	10.000	10.000	-0.997
1.0	2.0	0.05	-5.03334×10^{-1}	-5.03335×10^{-1}	2×10^{-4}	0.041	0.046	-0.033
		0.1	-5.13363×10^{-1}	-5.13363×10^{-1}	$< 1\times10^{-4}$	0.082	0.093	-0.067
		0.2	-5.53809×10^{-1}	-5.53809×10^{-1}	$< 1\times10^{-4}$	0.164	0.186	-0.135
		0.5	-8.51976×10^{-1}	-8.51992×10^{-1}	2×10^{-3}	0.424	0.470	-0.351
		1.0	-2.10739	-2.10825	4×10^{-2}	0.932	0.977	-0.738
		2.0	-8.00847	-8.00855	1×10^{-3}	1.995	2.003	-0.967
		5.0	-5.00013×10^{1}	-5.00013×10^{1}	$< 1\times10^{-4}$	5.000	5.000	-0.995
2.0	1.0	0.05	-1.00334	-1.00334	$< 1\times10^{-4}$	0.058	0.078	-0.033
		0.1	-1.01345	-1.01345	$< 1\times10^{-4}$	0.116	0.155	-0.067
		0.2	-1.05533	-1.05533	$< 1\times10^{-4}$	0.238	0.314	-0.138
		0.5	-1.43491	-1.43655	1×10^{-1}	0.712	0.857	-0.432
		1.0	-4.06678	-4.06746	2×10^{-2}	1.966	1.998	-0.875
		2.0	-1.60159×10^{1}	-1.60159×10^{1}	$< 1\times10^{-4}$	3.996	4.000	-0.969
		5.0	-1.00003×10^{2}	-1.00003×10^{2}	$< 1\times10^{-4}$	10.000	10.000	-0.995

We note that the ground–state energy is accurately given by the two–parameter ansatz and that the three–parameter ansatz does not significantly improve on these results. Furthermore an examination of the variational parameters for the two ansätze shows that $x_{1,\mathrm{opt}} \simeq x_{2,\mathrm{opt}} \simeq x_{\mathrm{opt}}$. This indicates

Table 4.5: *Comparison of the first excited state energy of the Rabi Hamiltonian obtained from a PBV calculation based on the odd–parity three–parameter ansatz (4.41),* E_1^{PBV3}*, with the results of a CI diagonalization in a basis of 101 odd–parity states,* E_1^{CI}*. Also shown are the percentage error* $\left|E_1^{\mathrm{PBV3}} - E_1^{\mathrm{CI}}\right| / E_1^{\mathrm{CI}} \times 100$*, and the values of the variational parameters* $x_{1,\mathrm{opt}}$*,* $x_{2,\mathrm{opt}}$*, and* v_{opt} *at the stationary point of the energy.*

ω_0	ω	g	E_1^{PBV3}	E_1^{CI}	% Error	$x_{1,\mathrm{opt}}$	$x_{2,\mathrm{opt}}$	v_{opt}
1.0	1.0	0.05	3.95108×10^{-1}	3.95102×10^{-1}	2×10^{-3}	0.119	0.316	-0.956
		0.1	2.80737×10^{-1}	2.80666×10^{-1}	2.5×10^{-2}	0.230	0.448	-0.922
		0.2	2.39619×10^{-2}	2.33675×10^{-2}	2.5	0.437	0.639	-0.877
		0.5	-1.00774	-1.01018	2.4×10^{-1}	1.005	1.097	-0.853
		1.0	-4.01643	-4.01658	3×10^{-3}	1.989	2.004	-0.936
		2.0	-1.60040×10^{1}	-1.60040×10^{1}	$< 1\times10^{-4}$	3.999	4.000	-0.984
		5.0	-1.00001×10^{2}	-1.00001×10^{2}	$< 1\times10^{-4}$	10.000	10.000	-0.997
1.0	2.0	0.05	4.90049×10^{-1}	4.90049×10^{-1}	$< 1\times10^{-4}$	0.055	0.071	-10.050
		0.1	4.60758×10^{-1}	4.60758×10^{-1}	$< 1\times10^{-4}$	0.109	0.140	-5.097
		0.2	3.50544×10^{-1}	3.50542×10^{-1}	5×10^{-4}	0.217	0.271	-2.680
		0.5	-2.71436×10^{-1}	-2.71650×10^{-1}	8×10^{-2}	0.526	0.603	-1.333
		1.0	-1.97098	-1.97218	6×10^{-2}	1.009	1.055	-0.983
		2.0	-8.00813	-8.00821	1×10^{-3}	1.995	2.003	-0.968
		5.0	-5.00013×10^{1}	-5.00013×10^{1}	$< 1\times10^{-4}$	5.000	5.000	-0.995
2.0	1.0	0.05	-1.61742×10^{-2}	-1.65009×10^{-2}	1.9	0.104	0.774	-0.110
		0.1	-6.29720×10^{-2}	-6.42075×10^{-2}	1.9	0.207	0.791	-0.212
		0.2	-2.31762×10^{-1}	-2.35841×10^{-1}	1.7	0.405	0.849	-0.379
		0.5	-1.14872	-1.15708	7×10^{-1}	0.966	1.147	-0.658
		1.0	-4.06603	-4.06664	2×10^{-2}	1.969	2.000	-0.875
		2.0	-1.60159×10^{1}	-1.60159×10^{1}	$< 1\times10^{-4}$	3.996	4.000	-0.969
		5.0	-1.00003×10^{2}	-1.00003×10^{2}	$< 1\times10^{-4}$	10.000	10.000	-0.995

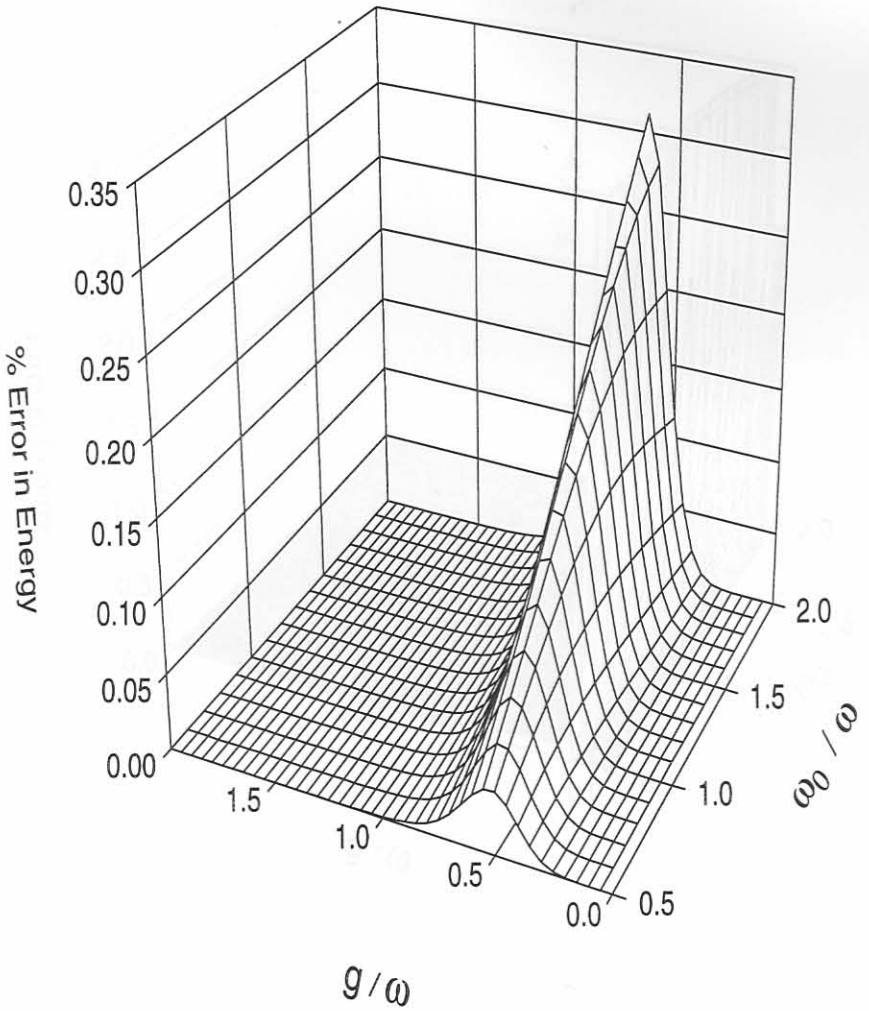

Figure 4.7: *The percentage error in the ground–state energy of the Rabi Hamiltonian obtained from the even–parity three–parameter PBV ansatz (4.41),* E_0^{PBV3}, *compared to the results of a CI diagonalization in a basis of 101 even–parity states, as a function of the coupling* g/ω *and the two–level splitting* ω_0/ω.

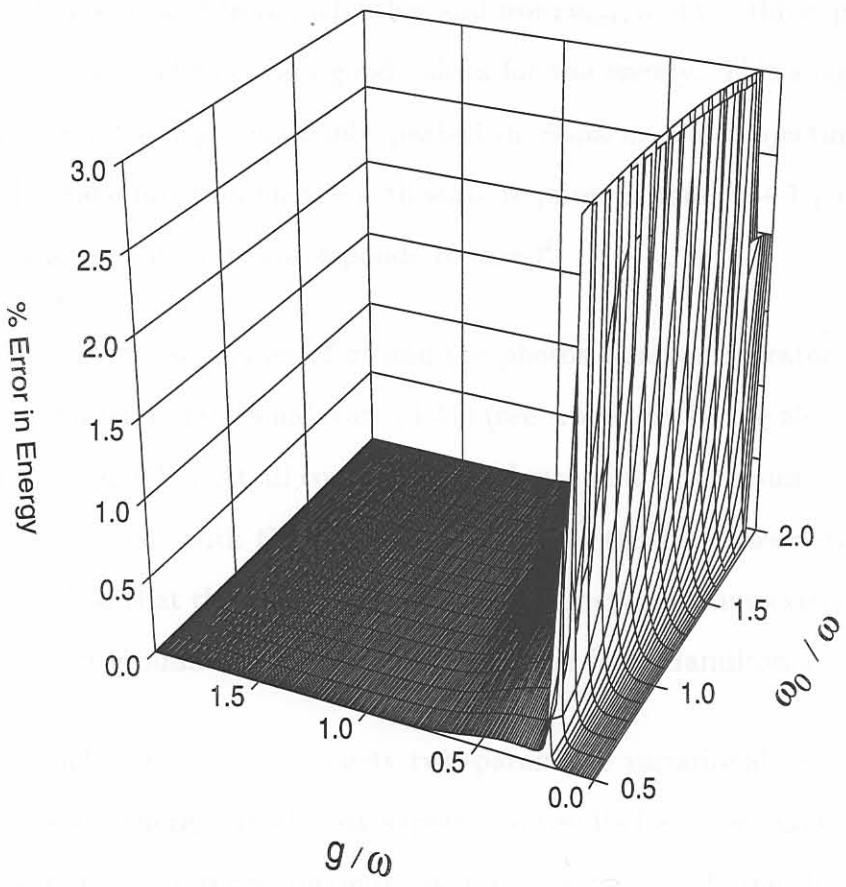

Figure 4.8: *The percentage error in the first excited state energy of the Rabi Hamiltonian obtained from the odd–parity three–parameter PBV ansatz (4.41),* E_1^{PBV3}*, compared to the results of a CI diagonalization in a basis of 101 odd–parity states, as a function of the coupling* g/ω *and the two–level splitting* ω_0/ω*. Note that we have had to truncate the plot in the vertical direction since one obtains an infinite percentage error when the energy becomes zero.*

that the ground state is a singly peaked function in x-space. The same is certainly not true for the first excited state where $x_{1,\mathrm{opt}}$ and $x_{2,\mathrm{opt}}$ are significantly different both from each other and from x_{opt}, and the three–parameter ansatz is essential to obtain good values for the energy. This suggests that the first excited state is doubly peaked in x-space. We conjecture [Bi99a] that the wave function for the n-th state requires in total $n+1$ parameters, where the ground state corresponds to $n=1$.

The expectation values of σ^z and the photon number operator $b^\dagger b$ in the three–parameter variational state (4.41) (see Appendix C) are also plotted in Figures 4.5 and 4.6. At all couplings, the three–parameter results are in even better agreement with the diagonalization than the two–parameter results, and it is clear that the three–parameter wave function is thus extremely close to the exact ground–state wave function of the Rabi Hamiltonian.

In conclusion, our even–parity two–parameter variational results for the ground–state energy are already superior to results (see, *e.g.* [Qi98, Wo96b]) obtained via other approximate many–body techniques. Using the computationally inexpensive three–parameter variational calculation, we obtain even better results for both the energies and wave functions of the ground and first excited states of the Rabi system. This calculation therefore provides a benchmark of simplicity and accuracy against which other methods, such as the CCM, may be measured.